Synthesis of ultrasmall metal nanoparticles and continuous shells at the liquid/liquid interface in Ouzo emulsions

Olivier Gazil, Nick Virgilio, Fabienne Gauffre

COMMUNICATION

Synthesis of Ultrasmall Metal Nanoparticles and Continuous Shells at the Liquid/Liquid Interface in Ouzo Emulsions

Received 00th January 20xx,

Accepted 00th January 20xx

DOI: 10.1039/x0xx00000x

Olivier Gazil,*[a, b] Nick Virgilio [b] and Fabienne Gauffre [a]

Herein, we report a novel method to synthesize metal nanoparticle-shells (NP-shells) and continuous shells at the liquid/liquid interface, via an interfacial reaction in an Ouzo emulsion. Ouzo emulsions spontaneously form submicronic droplets with a narrow size distribution, without any energy-intensive process. The Ouzo system in this work comprises water, tetrahydrofuran (THF) and butylated hydroxytoluene (BHT), and forms BHT-rich droplets (~100 nm). The addition of a reducing agent ($NaBH_4$) in the aqueous phase, and of a metal precursor ($AuPPh_3Cl$ and/or $Pd(PPh_3)_2Cl_2$) in the BHT-rich droplets, results in the formation of Au nanoparticles (AuNPs), continuous Pd shells, or bimetallic shells, at the interface of the droplets. Control over the NP-shells size was achieved by the addition of a water-soluble polymer during the synthesis, which in turn leads to smaller NP-shells.

In nature, hollow nanocapsules (i.e. vesicles) are abundant and associated to many biological functions such as digestion, transport, and storage.[1] Synthetic equivalents of these materials, such as colloidosomes (i.e. microcapsules whose shells are formed with micro- or nanoparticles (NPs)), have been largely studied for high value applications ranging from encapsulation, imaging, therapy, batteries, and catalysis, as well as for the development of metamaterials.[2-9] The interest of spherical nano-objects stabilized by particles was already demonstrated at different scales: Pickering emulsions (~µm), armored bubbles (~10 µm) and liquid marbles (~mm). Indeed, Pickering emulsions and armored bubbles are much more stable than their counterparts stabilized by surfactants.[10, 11] Liquid marbles can only be prepared using particles and show very interesting non-adhesive properties.[12]

Another approach to synthesize these objects is the Ouzo effect, which leads to the spontaneous formation of droplets. Introduced by Vitale and Katz, the typical example of the Ouzo effect is when an anis-based alcohol, such as Pastis or Ouzo, is added to water, producing a cloudy solution – the result of *trans*-anethol nanoprecipitation caused by its low solubility in water.[13] Interestingly, this precipitation yields metastable and nearly monodisperse sub-µm droplets (typically 100-300 nm).[13-15] In the same way that conventional emulsions can be used as templates for the synthesis of colloidosomes, it has been shown that NPs adsorb at the surface of Ouzo emulsion droplets, and limit the coalescence of droplets.[14-16] Thus, Ouzo emulsions stabilized with nanoparticles share similarities with Pickering emulsions, in which particles act as surfactant.[11] However, in contrast with Ouzo emulsions stabilized with particles, Pickering emulsions yield micron-sized droplets or larger, and the formation and stabilization of sub-µm droplets have yet to be generalized.[3, 17-19] Furthermore, Pickering emulsions also typically require energy intensive processes complicating their development at the industrial scale.[14, 17] These two types of emulsions are different from a fundamental point of view: traditional emulsification is a top-down approach (the oil phase is fractionated from bulk into droplets) while Ouzo emulsification is a bottom-up approach (the oil phase nucleates from the solvated state to droplets), leading to several differences in their outcomes.

In the vast majority of examples, the liquid/liquid interfaces are coated by preformed NPs, initially dispersed in one of the liquid phases. In contrast, reports on the *in situ* synthesis of NPs directly at the interface in emulsion-based systems remain scarce. López-de-Luzuriaga et al. reported a single-step AuNPs synthesis by reducing a gold complex with triisopropylsilane at the interface of oleic acid droplets,[2] while Sachdev et al. detailed the synthesis of AuNPs at the interface of hexane droplets (formulated in a microfluidic chip) with decamethylferrocene,[20] and Li et Zhang described the formation of Fe_3O_4 nanoshells on the surface of gas bubbles under hydrothermal conditions (i.e. armored bubbles).[21] In addition, several articles report on the seeded growth of NPs at the interface from an already formed Pickering emulsion.[3, 22]

[a] Univ Rennes, CNRS, ISCR-UMR6226, F-35000 Rennes, France. E-mail: olivier.gazil@polymtl.ca

[b] CREPEC, Department of Chemical Engineering, Polytechnique Montréal, C.P. 6079 Succursale Centre-Ville, Montréal, Québec H3C 3A7, Canada.

[c] †Electronic Supplementary Information (ESI) available: Experimental sections, tables, figures, and tomography video. See DOI: 10.1039/x0xx00000x

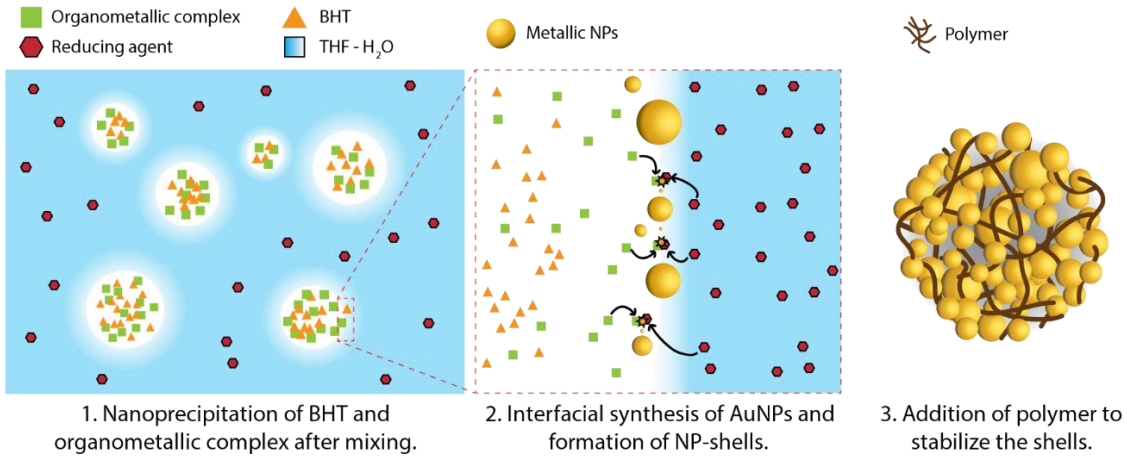

Scheme 1. Synthesis of AuNPs at the liquid/liquid interface in Ouzo-type emulsions, and immobilization of AuNPs at the interface with a strongly adsorbing polymer.

Among the different pathways employed to locally synthesize particles at the liquid/liquid interface, the approach developed by Rao et al. is a promising candidate.[23] It involves an aqueous phase comprising a reducing agent, and an organic phase containing a metallic precursor. The reactants can be chosen to yield a variety of metals (e.g. Au, Ag and Pd), oxides (e.g. CuO and ZnO) and chalcogens (e.g. CuS and CdS) 2D thin films.[23] This approach was subsequently used by Gazil et al. to cover complex hydrogel structures with a thin metal film,[24] and by Armstrong et al. to cover emulsified toluene droplets with metal NPs.[25] However, to the best of our knowledge, it was never used in combination with an Ouzo-type emulsion. We expect that the synthesis of NPs at the surface of Ouzo droplets will stabilize them and allow control over their sizes, leading *in fine* to the formation of NP-shells (i.e. hollow spheres composed of NPs). Essentially, our results demonstrate that interfacial reactions can be employed in Ouzo and other emulsion-type systems to synthesize ultrasmall metal nanoparticles and thin shells at the interface – a promising pathway to synthesize a wide variety of new materials, owing to the simplicity and reproducibility of the method.

In this work, we take advantage of Ouzo emulsions to achieve an interfacial reduction of metallic precursors and coat submicronic droplets with metal nanostructures.[23] The Ouzo system comprises butylated hydroxytoluene (BHT, a stabilizer added to tetrahydrofuran, THF), and water. The proposed reaction mechanism for the interfacial reaction – hereafter designated as *in situ* synthesis – is presented in Scheme 1. For the sake of clarity, the various steps are presented in chronological order, though they are in fact happening simultaneously. First, an aqueous phase comprising a reducing agent (sodium borohydride – $NaBH_4$) is mixed with an organic phase (THF) containing a metallic precursor ($AuPPh_3Cl$) and BHT. This leads to the fast nanoprecipitation of BHT with the precursor (they are both hydrophobic), while the reducing agent remains in the aqueous phase. Second, the redox reaction between the reducing agent and the organometallic complex is initiated at the interface of the droplets, resulting in the formation of AuNPs. Finally, when the AuNPs are fully synthesized, a water-soluble polymer is added to stabilize, via adsorption, the AuNP-shells.

In a typical *in situ* synthesis, 0.75 mL of an aqueous solution containing 10 mM sodium borohydride ($NaBH_4$) is quickly added to 0.25 mL of a THF solution containing BHT (~320 ppm)[26] and 1.5 mM $AuPPh_3Cl$. The high excess of reducing agent versus precursor (20:1 molar ratio) ensures reaction completion in a short period of time. For this reason, sampling times at 1 min (~ at reaction completion) and 30 min were chosen for nanoparticle tracking analysis (NTA) and transmission electron microscopy (TEM) observations. First, TEM analysis revealed the formation of nearly spherical nano-objects formed by closely packed AuNPs, as Figure 1a (1 min) and 1b (30 min) show. High resolution TEM (HRTEM) micrographs are presented in Figure S1, and a micrograph showing individual AuNPs is presented in Figure S2a. No significant differences between the 1 min and 30 min syntheses were observed for the individual AuNPs (Table S1), thus only the 30 min synthesis is presented in Figure S2. The size distribution of the individual AuNPs composing the shells is presented in Figure S2b. The energy-dispersive X-ray spectroscopy (EDX) spectrum (Figure S2c) confirms the formation of AuNPs. AuNPs crystallinity can be observed on the HRTEM micrograph (Figure S2a) with the lattice fringes, which is also confirmed by selected area electron diffraction (SAED – Figure S2d). Hollowness of the NP-shells is shown in Figure S3, where a darker edge can be observed – the core is empty, as the lighter contrast in the center illustrates.

The comparison of Figure 1a and b reveals much larger NP-shells after 30 min of synthesis time, as compared to 1 min (note the difference between the two scales). Their respective size distributions, as obtained by NTA, are presented in Figure 1c. After 1 min reaction, the mean size of the NP-shells is 160 ± 50 nm, and the size distribution shows a main mode centered at 140 nm, sharp and narrow. In contrast, a reaction time of 30 min gives a polydisperse distribution with a mean of 300 ± 200 nm and a mode at 150 nm. Size analyses were also obtained based on the TEM micrographs (Figure 1d): after a reaction time of 1 min, the NP-shells average diameter is 160 ± 80 nm (polydispersity index PDI = 0.3), while it is 800 ± 400 nm after 30 min (PDI = 0.2). It is important to mention that NTA gives the

hydrodynamic diameter, which is expected to be larger than the geometrical size determined by TEM.[27] However, it is noteworthy to mention that objects larger than 1 µm are excluded from the NTA analysis, mainly because of their limited Brownian motion. This, combined with the time evolution of sample while solution dries on TEM grid, explains why here NP-shells observed by TEM are larger compared to NTA results. It is clear that the average diameter evolves with time between 1 min and 30 min of reaction time – the droplets are not stable and tend to coalesce. This is further supported by NTA measurements after 2 h of reaction time (Figure S4), and a picture of the sample in a vial after 1 day (Figure S5b-d) showing that almost all the NP-shells have coalesced and precipitated at the bottom of the vial. The NPs diameter evolution has an impact on two important factors: coverage and density of the objects. A single layer of 2.7 nm AuNPs around the Ouzo droplets would give the 1 min objects a coverage of 0.8, while it is 1.0 for the 30 min objects (Equation S1) – these numbers are a rough estimate of the coverage based on a few hypotheses (a value of 1 means full coverage). Even though the coverage is around 100%, coalescence is still present – it has been shown in the case of liquid marbles that the formation of holes between contacting spheres is easier for smaller particles.[12, 28] Furthermore, the density was measured as an indicator for sedimentation and a value of 2.1 was calculated for the 1 min AuNP-shells, as compared to 1.3 for the 30 min objects (Equation S2). Considering the important coalescence, it is thus required to properly stabilize the AuNP-shells for their storage and later use.

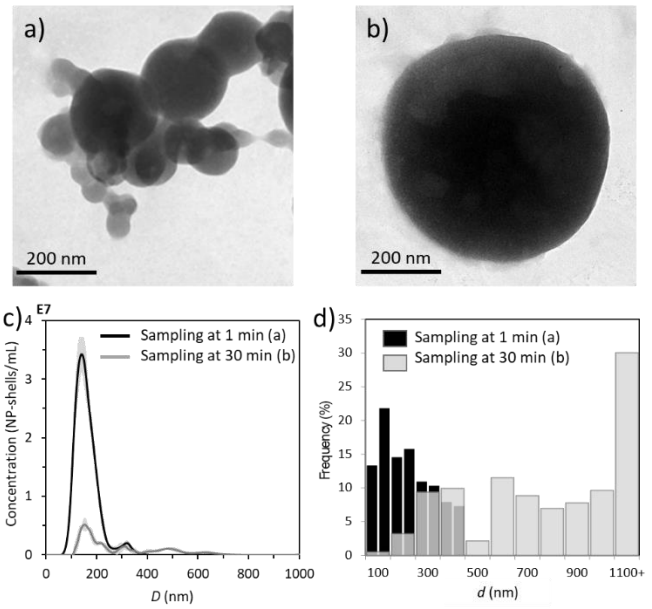

Figure 1. *In situ* synthesis of AuNPs at the interface of BHT-rich nanodroplets by the reduction of 0.25 mL of 1.5 mM $Au(PPh_3)Cl$ with 0.75 mL of 10 mM aqueous $NaBH_4$. TEM micrographs of the metallic NP-shells after reaction times of a) 1 min and b) 30 min. c) Size distributions of the NP-shells in solution for both samples as acquired by NTA (see methodology in ESI). d) Histogram of the dry samples obtained from the TEM micrographs.

One way to stabilize the shells against aging is by adding a polymer with functional groups that have an affinity for gold (e.g. amine or thiol groups).[29] Here, poly(allylamine hydrochloride) (PAA HCl) was selected as a potential stabilizer due to the affinity of amine groups with Au.[29] Adding 50 µL of a 4.4 mg/mL PAA HCl solution (equivalent to 0.75 mg polymer/mg Au) after 1 min of reaction time yields smaller objects (50 ± 20 nm) and less polydispersed (PDI = 0.1) as compared to the synthesis without polymer (Figure 2a). In addition, the NP-shells suspension remains stable over time against sedimentation. Aged samples stabilized by PAA HCl are displayed in Figure S6. The shells average size slightly increases after 2 weeks, from 50 nm to 70 nm (Figure S6c and Table S1). Furthermore, the individual AuNPs grow from 2.8 nm to 3.4 nm (Figure S6d and Table S1), which results in less homogeneous NP-shells (Figure S6a-b) as compared to the freshly prepared sample (Figure 2a). This increase remains quite limited, but this could indicate that the particles, while being properly stabilized by a polymer as a spherical assembly, can still interact and coalesce with neighboring AuNPs – hence, suggesting the fact that their surfaces are still active and accessible for potential catalysis applications, for example.

In comparison, AuNPs were also synthesized in bulk (by reducing the metal precursor with $NaBH_4$ in THF, designated as "*ex situ* synthesis"), then added to the Ouzo emulsion. Poly(vinylphosphonic acid) (PVPA) was also tested as a stabilizing polymer (50 µL of a 4.4 mg/mL PVPA), since PAA HCl led to the significant coalescence of AuNPs in that case (Figure S7). This result can be explained by zeta potential measurements. Repulsive forces are deemed strong enough to stabilize droplets when the absolute value of the zeta potential is above 30 mV. The initial Ouzo emulsion is quite stable (-37 ± 4), while the potential of droplets with AuNPs synthesized *in situ* is close to neutrality (0.43 ± 0.07). The addition of a polymer (PAAH) increases the zeta potential of the AuNP-shells to 30 ± 2 and helps stabilize the droplets against coalescence due to the repulsive forces, which is consistent with previous observations.

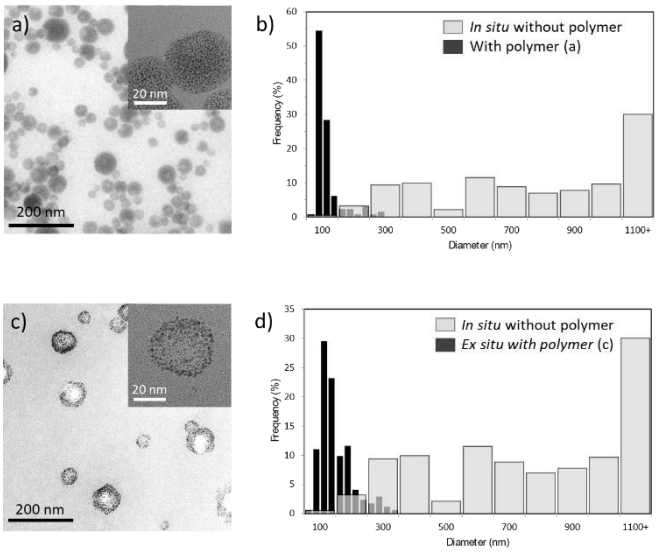

Figure 2. a) TEM micrographs of NP-shells (inset: HRTEM) synthesized *in situ* with 0.25 mL of 1.5 mM $Au(PPh_3)Cl$ and 0.75 mL of 10 mM aqueous $NaBH_4$, followed by the addition of 50 µL of 4.4 mg/mL PAA HCl after 1 min reaction time; b) corresponding histogram extracted from TEM micrographs in black, and without the addition of PAA

HCl in grey; c) micrographs of AuNPs synthesized in THF first (*ex situ* synthesis), followed by the addition of water, and of 50 µL of 4.4 mg/mL PVPA. d) Histograms of NP-shells synthesized *in situ* without PVPA (grey), compared to NP-shells with AuNPs synthesized *ex situ* and with the addition of PVPA. In both cases, the stabilizing effect of the polymer (PAA HCl in one case, and PVPA in the other) is significant.

Considering the *ex situ* synthesis, which is highly positive (46 ± 1), the addition of PVPA gives the droplets a negative charge (-54 ± 3), which is consistent with the observation that PVPA (a negatively charged polymer) stabilizes them, whereas PAA (positively charged) has not effect.

TEM and HRTEM micrographs in Figure 2c show *ex situ* synthesized AuNPs forming shells around droplets with the addition of 50 µL of 4.4 mg/mL PVPA, with the resulting histogram in Figure 2d. Clearly, this approach, combined with PVPA, also leads to a relatively narrow NP-shells size distribution (100 ± 40 nm and PDI = 0.1). However, shell coverage is not as homogeneous as for the *in situ* synthesis, since the AuNPs surface density appears to be lower. Unexpectedly, the average sizes of the individual AuNPs are quite similar for the *in situ* and *ex situ* approaches (respectively 2.7 ± 0.4 nm and 2.9 ± 0.6 nm, see Table S1). X-ray diffraction (XRD) was also performed for both syntheses (Figure S8) showing that they yield identical crystalline structure. From the Scherrer equation (Equation S3), the size of the crystallites can be calculated (1.6 nm) and compared to the size of the NPs measured with the TEM micrographs (2.7 nm and 2.9 nm, see Table S1), confirming their similarities. This suggests that the reduction of the gold precursor is only weakly sensitive to the local conditions (interfacial versus bulk). This may be due to the high concentration and the strength of the reducing agent used (20:1 ratio of reducing agent per metallic precursor).

Different applications may require different types of metal NPs (e.g. for catalysis, palladium or Au/Pd alloys are also of interest).[5, 30-32] For this reason, using a palladium precursor with the same triphenylphosphine ligands ($Pd(PPh_3)_2Cl_2$) was assessed. Instead of discrete NPs, the reduction of the Pd precursor yielded a continuous and amorphous Pd shell (Figure3a, and Figure S1e for higher magnification). The addition of a polymer (PVPA) was studied as well (Figure S9).

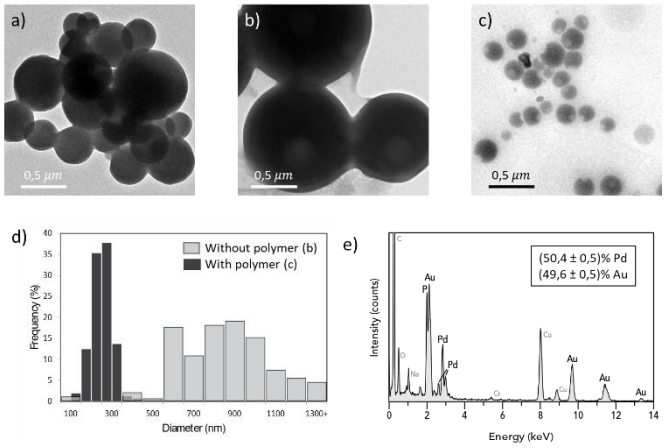

Figure 3. a) TEM micrograph of continuous shells synthesized *in situ* with 0.25 mL of 1.5 mM $Pd(PPh_3)_2Cl_2$ and 0.75 mL of 10 mM aqueous $NaBH_4$ (average size of 500 ± 200 nm). b-c) Shells composed of an equimolar Au-Pd ratio, showing the thin layer synthesized *in situ* (with 0.75 mM of $Pd(PPh_3)_2Cl_2$ and $Au(PPh_3)Cl$): TEM micrographs without (b) and with (c) the addition of 50 µL of 4.4 mg/mL PAA HCl after 1 min of reaction time; d) histograms of both samples displayed in (b) and (c), obtained by image analysis; e) EDX spectra of (b) and (c) (both spectra are almost identical) highlighting the expected compositions in Au and Pd – i.e., 50/50 mol%. Identified in black are peaks associated to both Au and Pd, with the phosphorous peak. Identified in grey, the elements composing the sample holder and the grid, plus non-relevant elements (e.g. Na of the reducing agent).

While it does reduce the average objects size and narrows the distribution, from 500 ± 200 nm (PDI = 0.1) down to 410 ± 90 nm (PDI = 0.05), its effect is more limited compared to the *in situ* AuNP-shells synthesis. A complementary *in situ* synthesis was performed by using exclusively the palladium precursor, without BHT. This synthesis yielded Pd-based objects (with a diameter of 180 ± 30 nm) displaying an increased stability of over several months (Figure S10). In the case of an equimolar combination of Au and Pd, bimetallic shells were obtained. Figure 3 shows bimetallic shells without (b) and with (c) the addition of 50 µL of 4.4 mg/mL PAA HCl. Again, there is a clear stabilizing effect of the polymer, as confirmed by the TEM micrographs and the histogram in Figure 3d. For similar synthesis conditions, the addition of PAA HCl inhibits NP-shells coalescence (800 ± 200 nm without PAA HCl, down to 200 ± 40 nm with the polymer). EDX analysis confirms the bimetallic composition of the shells (Figure 3e). Indeed, the integration of the peaks for Au and Pd gives the expected molar composition – i.e. 50/50 mol% (the initial precursors were added in equimolar amounts). Furthermore, the phosphorus signal is more intense as compared to pure AuNP-shells (Figure S2c), which is caused by the initial Pd complex possessing twice the amount of triphenylphosphine groups per metal atom. HRTEM observations of the Au/Pd shells are shown in Figure 3b and Figure S1f (without PAA HCl): nanoparticles appear to be embedded in a matrix. From the previous observations for the pure Au and pure Pd precursors, it seems that the structure consists of AuNPs embedded in a matrix of Pd. In contrast to gold, the *in situ* and *ex situ* (Figure S11) syntheses yield two very different results for the Pd precursor.

The formation of a dense layer of NPs that coat the droplet, as it is the case when $Au(PPh_3)Cl$ is reduced at the interface, is reminiscent of Pickering emulsions. However, it should be noted that ultra-small particles are formed here. In fact, these are amongst the smallest particles reported at the fluid/fluid interface in emulsion-type systems (the typical size usually reported is around 0.01-10 µm).[3, 4, 17-19] In the case of Pickering emulsions, droplet coalescence is limited by the particle layer and stops when the total amount of interface matches the coating ability of the particles.[11, 15, 33] The same mechanism was also demonstrated recently for spontaneous Ouzo emulsions using particles of ~8 nm.[15] In order to separate the stabilizing effect of the NPs on the droplets (i.e. Pickering emulsion), from the effect of the polymer, the growth of the droplets in the presence of the polymer was monitored by DLS (Figure S12). The results show that with and without polymer, the droplet size stabilizes around the same value (ca 600 nm) over the typical reaction time (< 30min) – i.e. the polymer alone does not particularly inhibit coarsening. Coarsening was also observed for droplets covered only with NPs (Figure S4). Consequently, both the NPs and polymer must be combined to stabilize the

NP-shells against coalescence. This significantly improves the lifetime of basic Ouzo emulsions (typically limited to hours, or days at most).[34] It is also noteworthy to underline the structural integrity of the NP-shells even after drying, highlighted by the 3D structure shown by TEM-tomography in the ESI video. Finally, an interesting observation is the presence of a hole on all shells (a few examples are highlighted in Figure S13, and it is illustrated in the ESI tomography video), regardless of their sizes, which may be an artifact due to the drying preparation step prior to TEM observations. This phenomenon was also observed in a previous work investigating the formation of spherical polysaccharide-based nanoparticles, specifically when using THF as the solvent.[35]

In conclusion, the *in situ* interfacial reduction of an organometallic precursor in Ouzo-type emulsions yield metal shells comprised of ultrasmall AuNPs, Pd continuous shells, or a combination of both in bimetallic systems, in a one-pot approach. The elaboration of such ultrasmall nanoparticles assemblies at the liquid/liquid interface is quite challenging since their adsorption is not as energetically favorable as for larger ones, explaining why reports for these types of particles are scarce.[36] Here, the addition of an appropriate polymer stabilizes the NP-shells and reduce their final sizes. To further reduce polydispersity, additional purification steps could be considered, depending on the application. Yet, the simplicity of the process makes it appealing, for example, for applications in therapeutics or catalysis.[2-6] Future work will aim at providing insight into the impact of metallic precursors on the Ouzo droplets size and stability, and at generalizing the approach to other metal-based systems, in order to better understand and control the synthesis of those materials.

Acknowledgements

This work was supported by the Alexander Graham Bell Canada graduate scholarships program from the Natural Sciences and Engineering Research Council of Canada (NSERC), from the ANR (ANR-20-CE06-0031-01 OUZOFAN), and from the IRN Nanomatériaux Multifonctionnels Contrôlés (IRN NMC). Prof. Virgilio acknowledges the financial support of NSERC via the Discovery Grants program. The authors would like to acknowledge support from Ludivine Rault for the assistance in TEM characterizations performed on THEMIS platform (ScanMAT, UAR 2025 University of Rennes 1-CNRS; CPER-FEDER 2007–2014) and Dr. Mathieu Pasturel for XRD characterizations. We finally thank Dr. Clément Goubault for helping in the laboratory with the methods developed by Dr. Gauffre's research group and Déborah Iglicki for a fruitful collaboration concerning *ex situ* synthesis.

Conflicts of interest

There are no conflicts to declare.

Notes and references

1 A. Morshed, B. I. Karawdeniya, Y. N. D. Bandara, M. J. Kim and P. Dutta, *Electrophoresis*, 2020, **41**, 449-470.
2 J. M. López-de-Luzuriaga, M. Monge, J. Quintana and M. Rodríguez-Castillo, *Nanoscale Advances*, 2021, **3**, 198-205.
3 L. Zhang, Q. Fan, X. Sha, P. Zhong, J. Zhang, Y. Yin and C. Gao, *Chem Sci*, 2017, **8**, 6103-6110.
4 K. L. Thompson, M. Williams and S. P. Armes, *J Colloid Interface Sci*, 2015, **447**, 217-228.
5 M. Pera-Titus, L. Leclercq, J.-M. Clacens, F. De Campo and V. Nardello-Rataj, *Angewandte Chemie International Edition*, 2015, **54**, 2006-2021.
6 F. J. Rossier-Miranda, C. G. P. H. Schroën and R. M. Boom, *Colloids and Surfaces A: Physicochemical and Engineering Aspects*, 2009, **343**, 43-49.
7 L. Dang, H. Ma, J. Xu, Y. Jin, J. Wang, Q. Lu and F. Gao, *CrystEngComm*, 2016, **18**, 544-549.
8 J. Jiang, G. Nie, P. Nie, Z. Li, Z. Pan, Z. Kou, H. Dou, X. Zhang and J. Wang, *Nano-Micro Letters*, 2020, **12**, 183.
9 C. Goubault, U. Jarry, M. Bostoën, P.-A. Éliat, M. L. Kahn, R. Pedeux, T. Guillaudeux, F. Gauffre and S. Chevance, *Nanomedicine: Nanotechnology, Biology and Medicine*, 2022, **40**, 102499.
10 A. Cervantes Martinez, E. Rio, G. Delon, A. Saint-Jalmes, D. Langevin and B. P. Binks, *Soft Matter*, 2008, **4**, 1531-1535.
11 B. P. Binks, *Current Opinion in Colloid & Interface Science*, 2002, **7**, 21-41.
12 B. P. Binks, S. K. Johnston, T. Sekine and A. T. Tyowua, *ACS Appl Mater Interfaces*, 2015, **7**, 14328-14337.
13 S. A. Vitale and J. L. Katz, *Langmuir*, 2003, **19**, 4105-4110.
14 G. Francois and J. L. Katz, *Chemphyschem*, 2005, **6**, 209-216.
15 C. Goubault, D. Iglicki, R. A. Swain, B. F. P. McVey, B. Lefeuvre, L. Rault, C. Nayral, F. Delpech, M. L. Kahn, S. Chevance and F. Gauffre, *J Colloid Interface Sci*, 2021, **603**, 572-581.
16 F. Sciortino, G. Casterou, P.-A. Eliat, M.-B. Troadec, C. Gaillard, S. Chevance, M. L. Kahn and F. Gauffre, *ChemNanoMat*, 2016, **2**, 796-799.
17 C. Albert, M. Beladjine, N. Tsapis, E. Fattal, F. Agnely and N. Huang, *J Control Release*, 2019, **309**, 302-332.
18 J. Xiao, Y. Li and Q. Huang, *Trends in Food Science & Technology*, 2016, **55**, 48-60.
19 A. M. Bago Rodriguez and B. P. Binks, *Current Opinion in Colloid & Interface Science*, 2019, **44**, 107-129.
20 S. Sachdev, R. Maugi, J. Woolley, C. Kirk, Z. Zhou, S. D. R. Christie and M. Platt, *Langmuir*, 2017, **33**, 5464-5472.
21 Z. W. Li and Z. H. Yang, *Journal of Magnetism and Magnetic Materials*, 2015, **387**, 131-138.
22 X. Zhu, S. Zhang, L. Zhang, H. Liu and J. Hu, *RSC Advances*, 2016, **6**, 58511-58515.
23 C. N. R. Rao, G. U. Kulkarni, P. J. Thomas, V. V. Agrawal and P. Saravanan, *The Journal of Physical Chemistry B*, 2003, **107**, 7391-7395.
24 O. Gazil, T. Gancheva, M. Bilodeau-Calame, B. D. Favis and N. Virgilio, *Nanoscale Advances*, 2020, **2**, 5263-5270.
25 O. L. Armstrong, S. N. Baxter, F. L. Deepak and P. J. Thomas, *Chem Commun (Camb)*, 2020, **56**, 4801-4803.
26 C. Goubault, F. Sciortino, O. Mongin, U. Jarry, M. Bostoën, H. Jakobczyk, A. Burel, S. Dutertre, M.-B. Troadec, M. L. Kahn, S. Chevance and F. Gauffre, *Journal of Controlled Release*, 2020, **324**, 430-439.
27 V. Filipe, A. Hawe and W. Jiskoot, *Pharm Res*, 2010, **27**, 796-810.
28 C. Planchette, A. L. Biance and E. Lorenceau, *EPL (Europhysics Letters)*, 2012, **97**.

29 A. Heuer-Jungemann, N. Feliu, I. Bakaimi, M. Hamaly, A. Alkilany, I. Chakraborty, A. Masood, M. F. Casula, A. Kostopoulou, E. Oh, K. Susumu, M. H. Stewart, I. L. Medintz, E. Stratakis, W. J. Parak and A. G. Kanaras, *Chem Rev*, 2019, **119**, 4819-4880.
30 A. Biffis, P. Centomo, A. Del Zotto and M. Zecca, *Chemical Reviews*, 2018, **118**, 2249-2295.
31 L. Liu and A. Corma, *Chemical Reviews*, 2018, **118**, 4981-5079.
32 M.-C. Daniel and D. Astruc, *Chemical Reviews*, 2004, **104**, 293-346.
33 S. Arditty, C. P. Whitby, B. P. Binks, V. Schmitt and F. Leal-Calderon, *Eur Phys J E Soft Matter*, 2003, **11**, 273-281.
34 S. Prévost, S. Krickl, S. Marčelja, W. Kunz, T. Zemb and I. Grillo, *Langmuir*, 2021, **37**, 3817-3827.
35 E. Aschenbrenner, K. Bley, K. Koynov, M. Makowski, M. Kappl, K. Landfester and C. K. Weiss, *Langmuir*, 2013, **29**, 8845-8855.
36 Y. Lin, H. Skaff, T. Emrick, A. D. Dinsmore and T. P. Russell, *Science*, 2003, **299**, 226-229.

